

---

This is an electronic reprint of the original article.  
This reprint may differ from the original in pagination and typographic detail.

Ahmad, Zeeshan; Kaario, Ossi; Karimkashi, Shervin; Qiang, Cheng; Vuorinen, Ville; Larmi, Martti

**Effects of ethane addition on diesel-methane dual-fuel combustion in a heavy-duty engine**

*Published in:*  
Fuel

*DOI:*  
[10.1016/j.fuel.2020.119834](https://doi.org/10.1016/j.fuel.2020.119834)

Published: 01/04/2021

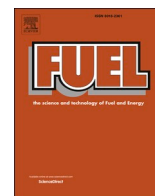
*Document Version*  
Publisher's PDF, also known as Version of record

*Published under the following license:*  
CC BY

*Please cite the original version:*  
Ahmad, Z., Kaario, O., Karimkashi, S., Qiang, C., Vuorinen, V., & Larmi, M. (2021). Effects of ethane addition on diesel-methane dual-fuel combustion in a heavy-duty engine. *Fuel*, 289, Article 119834.  
<https://doi.org/10.1016/j.fuel.2020.119834>

---

This material is protected by copyright and other intellectual property rights, and duplication or sale of all or part of any of the repository collections is not permitted, except that material may be duplicated by you for your research use or educational purposes in electronic or print form. You must obtain permission for any other use. Electronic or print copies may not be offered, whether for sale or otherwise to anyone who is not an authorised user.



# Effects of ethane addition on diesel-methane dual-fuel combustion in a heavy-duty engine

Zeeshan Ahmad<sup>\*</sup>, Ossi Kaario, Shervin Karimkashi, Cheng Qiang, Ville Vuorinen, Martti Larmi

Department of Mechanical Engineering, Aalto University, School of Engineering, 02150 Espoo, Finland

## ARTICLE INFO

### Keywords:

Experimental, numerical and theoretical studies  
Dual/Tri fuel  
Ethane-methane mixtures  
Natural gas composition  
Exhaust emissions

## ABSTRACT

The present study is a continuation of the previous work by Ahmad et al. (2020), in which ethane (C<sub>2</sub>H<sub>6</sub>) enriched diesel-methane (CH<sub>4</sub>) dual-fuel (DF) combustion was experimentally investigated in a single-cylinder heavy-duty engine. Here, the experiments of ethane enriched DF combustion are carried out with new details together with supporting zero-dimensional (0D) and one-dimensional (1D) chemical kinetics simulations. Three port-fuel injected (PFI) gaseous blends of pure methane with varying ethane concentrations of 0%, 10%, and 20% are used as the main fuels. The PFI gaseous blend provides 97% of the total-fuel energy (TFE), which is ignited by a small 3% (TFE based) pilot diesel. Experiments are performed under lean condition ( $\phi_{\text{gas}} = 0.52$ ) for two engine speeds while keeping the TFE and other operating conditions constant. Calculated results from 0D and 1D simulations under engine relevant conditions including theoretical combustion mode analysis ( $\beta$ -curve) are used to deepen the phenomenological understanding of the experimental results. The results reveal that adding ethane into pure methane has minor effects on the pilot-diesel ignition timing. However, ethane addition greatly enhances the ignitability of methane after the start of combustion. Ethane enriched gaseous blends yield higher thermal efficiency and reduce combustion duration compared to pure methane. According to combustion mode analysis, ethane tendency to promote spontaneous autoignition may be one of the reasons for improving overall combustion performance. It is observed that ethane enriched gaseous blends produce lower unburned methane (UB-CH<sub>4</sub>) and unburned hydrocarbons (THC) accompanied with higher nitrogen oxides (NO<sub>x</sub>) because of the higher combustion efficiency. Furthermore, ethane addition considerably helps to reduce cycle-to-cycle variations under lean conditions compared to pure methane.

## 1. Introduction

Natural gas (NG) as a low-carbon gaseous fuel is potentially a feasible alternative fuel for use in internal combustion engines, especially in diesel engines to meet stringent emission regulations [1–3]. It is mainly composed of methane (CH<sub>4</sub>) along with other heavier alkanes such as ethane (C<sub>2</sub>H<sub>6</sub>) and propane (C<sub>3</sub>H<sub>8</sub>) as well as diluents (N<sub>2</sub> and CO<sub>2</sub>). The composition of natural gas is highly dependent on the geographical location. However, it essentially contains at least 80% methane content regardless of the origin. Methane is a clean burning fuel, which produces low greenhouse gas (GHG) emissions due to its low C/H ratio [4]. However, it is still a fossil fuel like diesel and gasoline, which may restrict its consumption considering the future GHG goals in transport sector. In this scenario, biomethane produced from renewable energy sources can replace fossil natural gas, while maintaining the net GHG emissions to zero [5]. However, efficient burning of pure methane in

diesel engines is another challenge due to its high autoignition energy requirement [6,7].

Dual-fuel (DF) concept is one of the low-temperature combustion technologies, which enables the utilization of natural gas (methane) in already existing diesel engines. In these engines, a directly-injected small pilot diesel provides an ignition source for the port-fuel injected premixed methane-air mixture [6–8]. Shipping and power generation industries have already adopted such natural gas operated DF engines. These provide high thermal efficiency compared to baseline diesel engines at high loads [9]. In addition, they produce lower nitrogen oxides (NO<sub>x</sub>) and particulate matter (PM) under lean conditions [9]. However, under lean conditions while utilizing small pilot quantities, DF engines have the drawback of emitting total-unburned hydrocarbons (THC) and unburned CH<sub>4</sub> or ‘methane slip’ (UB-CH<sub>4</sub>) [10–12]. The global warming potential of methane is dramatically higher (~28 times) than CO<sub>2</sub> over long-term perspective [11,12]. Therefore, unburned CH<sub>4</sub> is a major concern in this context despite all the advantages of DF engines over

<sup>\*</sup> Corresponding author.

E-mail address: [zeeshan.ahmad@aalto.fi](mailto:zeeshan.ahmad@aalto.fi) (Z. Ahmad).

<https://doi.org/10.1016/j.fuel.2020.119834>

Received 31 August 2020; Received in revised form 1 November 2020; Accepted 20 November 2020

Available online 14 December 2020

0016-2361/© 2020 The Authors. Published by Elsevier Ltd. This is an open access article under the CC BY license (<http://creativecommons.org/licenses/by/4.0/>).

Nomenclature			
DF	Dual fuel	$\xi$	Mixture fraction
gIMEP	Gross indicated mean effective pressure	$\xi_{MR}$	Most reactive $\xi$
TDC	Top-dead center	$\xi_{St}$	Stoichiometric $\xi$
CAD	Crank angle degree	$Y'$	Level of stratification of mixture
ATDC	After top-dead center	$\lambda$	Spatial space of local mixture
HRR	Apparent heat release rate	$t_{ID}$	Ignition-delay time
AccQ	Accumulative heat release	$t_{comb}$	Combustion duration
TFE	Total injected-fuel energy	$\alpha$	Linear approx. for variation of $t_{ID}$ w.r.t. $\xi$
WI	Wobbe index	$\beta$	Parameter specifying combustion mode
MN	Methane number	$S_L, S_{ign}$	Laminar flame, ignition-wave speed
UB-CH <sub>4</sub>	Unburned methane or methane slip	$C_{input}$	Total carbon content of injected fuel
THC	Total unburned hydrocarbons	$T_{TDC}$	Calculated isentropic temperature at TDC
CO, CO <sub>2</sub>	Carbon mono-, di-oxide	$\phi_{gas}$	Gas/air equivalence ratio
NO <sub>x</sub>	Nitrogen oxides	$\eta_{comb}$	Combustion efficiency
$MP_{peak}$	Motored peak pressure (only air)	$\eta_{th}$	Thermal efficiency
I	First stage combustion	$\theta_{SOI}$	CAD at start of injection
II	Second stage combustion	$\theta_1, \theta_2, \theta_3$	CAD at start of combustion stages
III	Third stage combustion	$\theta_{3a}, \theta_{3b}$	CAD at start of high-, low-intensity regime of Stage III
$\dot{m}$	Mass flow rate	$\theta_{90}$	CAD where 90% of total heat releases

baseline diesel engines. It is thus important to further develop the lean DF combustion process in order to meet future GHG goals.

In past, several researchers have studied the impact of various natural gas compositions on combustion processes in IC engines [13]. Most of the studies present results either from spark-ignited engines [14,15] or from chemical modeling simulations along with validation data from shock-tube [16–18], rapid compression-expansion machine (RCEM) [18] or laboratory burner experiments [19,20]. All these studies state enhanced reactivity of natural gas due to the presence of heavier alkanes compared to pure methane. For instance, the presence of ethane in a gas blend is reported to improve spark-ignited engine performance and lean flammability limit [14,15]. Combined presence of ethane and propane in a gas blend is indicated to be beneficial for increasing fuel burning rate of lean mixtures [14,15]. Furthermore, heavier alkanes result in a shorter ignition-delay time and higher flame speed for homogeneous gas/air mixtures [17–19]. At temperatures below  $\sim 1100$  K, efficient production of methylperoxy ( $\text{CH}_3\text{O}_2$ ) and at high temperatures ( $>1300$  K), direct H-atom abstraction of heavier alkanes yield high concentration of OH radicals, which can improve ignition process of pure methane [16–18]. It is interesting to note that 4–8 cm/s faster laminar flame speed of natural gas (comprising  $< 20\%$  heavier alkanes) than homogeneous methane-air mixture is mainly due to the chemical kinetics effect [19,20].

Recently, there have been few numerical [21–23] and experimental [24,25] research works published regarding the implications of natural gas composition in DF engines. Mukulski et al. [21] investigated various blends of pure methane with varying concentrations of  $\text{C}_2\text{H}_6$ ,  $\text{C}_3\text{H}_8$ , and  $\text{C}_2\text{H}_6/\text{C}_3\text{H}_8$  in a DF engine using a zero-dimensional multiphase mathematical model. The results showed that diluting methane with  $\text{C}_2\text{H}_6$  has a reducing effect on ignition delay of diesel fuel, while with  $\text{C}_3\text{H}_8$  has a prolonging effect. Moreover, addition of equal volume of  $\text{C}_2\text{H}_6/\text{C}_3\text{H}_8$  (e.g. 10/10, 25/25) into pure methane does not affect ignition delay. On the other hand, numerical results (CFD-CONVERGE) by Wu et al. [22] revealed that adding  $\text{C}_2\text{H}_6$ ,  $\text{C}_3\text{H}_8$ , or  $\text{C}_2\text{H}_6/\text{C}_3\text{H}_8$  blends into methane/n-heptane mixtures shortens ignition-delay time at high temperatures while increases it at low-temperature range. Nevertheless, the presence of heavier alkanes is reported to shift the maximum heat release towards top-dead center (TDC) and burn the fuel faster than pure methane [21,22].

In our previous experimental work by Ahmad et al. [24], it was found that ignition-delay of pilot diesel reduces with 10%  $\text{C}_2\text{H}_6$  concentration

in a gas blend. However, it remains constant with further increase of  $\text{C}_2\text{H}_6$  concentration. It was concluded that ethane addition drastically reduces unburned  $\text{CH}_4$  and THC emissions accompanied with a significantly reduced level of cyclic variability. Apart from this, McTaggart-Cowan et al. [25] investigated directly injected non-premixed DF mode experimentally with a range of natural gas compositions in a heavy-duty engine. They directly injected gaseous fuel 1.0 ms after the end of diesel injection and demonstrated that heavier alkane addition to pure methane jet reduces THC at an expense of increased soot emissions.

Based on the aforementioned discussion, although it is known that the intrinsic presence of heavier alkanes in natural gas enhances its reactivity; their burning characteristics in DF engines are not well understood. Moreover, there is an experimental research gap to address the inconsistencies of numerical results especially in the context of DF combustion. Thus, while considering the future GHG emission goals, ethane (second simplest and most abundant component of natural gas) enriched diesel-methane DF combustion is investigated in this study experimentally under lean conditions with a small pilot at two engine speeds in a single-cylinder heavy-duty engine. In addition, zero-dimensional (0D) and one-dimensional (1D) numerical simulations together with combustion mode analysis are performed to deepen understanding of experimental results, phenomenologically. The objectives of the current work are:

1. to define DF combustion stages from heat release rate (HRR) profile,
2. to demonstrate the influence of engine speed on lean DF combustion characteristics and engine-out emissions,
3. to explain the influence of ethane enrichment on lean diesel-methane DF combustion performance and its burning characteristics including engine-out emissions,
4. to complement the experimental results with 0D and 1D numerical simulations and determine possible changes in the mode of combustion propagation by adding ethane.

## 2. Experimental setup and methods

### 2.1. Laboratory engine

In this work, a single-cylinder DF research engine is used for experiments. Fig. 1 shows a schematic of the laboratory-engine setup and Table 1 outlines the relevant specifications of the engine. The engine is

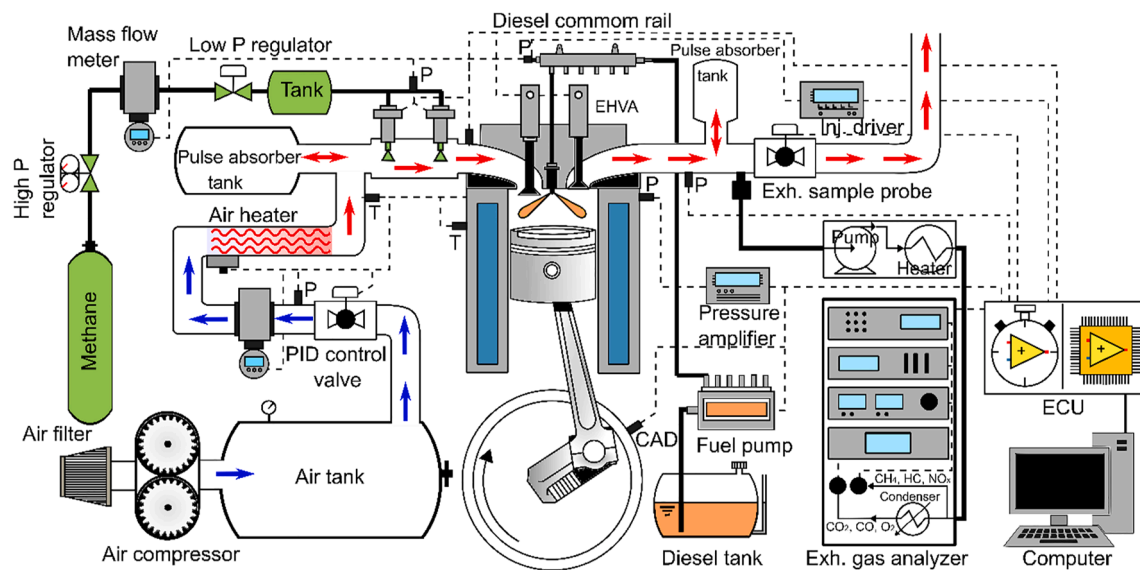


Fig. 1. Laboratory research-engine setup.

**Table 1**  
Test engine specifications.

Engine type	4 Stroke, modified single-cylinder DF engine		
Piston geometry	Re-entrant bowl		
Displacement volume	1.4 L		
Bore × Stroke	111 × 145 mm		
Geo. compression ratio	16.7:1		
In-cylinder swirl ratio	2.7		
Pilot injection system	Bosch common rail with piezoelectric injector		
Injector no. of holes × diameter	3 × 0.160 mm (symmetric)		
Port fuel injection system	2 × EG2000 gas injectors		
Firing TDC	0 CAD ATDC		
Valve timing		Inlet	Exhaust
	Opening time	356 CAD ATDC	150 CAD ATDC
	Closing time	−155 CAD ATDC	−340 CAD ATDC

coupled with necessary auxiliary systems such as electro-hydraulic valve actuation (EHVA), charge-air, direct and port-fuel injection systems, as well as exhaust emission analyzers and engine control unit. EHVA enables camshaft-less valve actuation with adjustable valve timings and lifts. The charge-air system is equipped with a compressor, air heater, and RHM-08 Coriolis mass flow meter (Rheonik Messtechnik GmbH, Accuracy: <0.1% of flow), providing charge air into the cylinder at a desired flow rate, temperature, and pressure. Similarly, the port-fuel injection system consisting of two gas injectors and RHM-015 Coriolis mass flow meter (Rheonik Messtechnik GmbH, Accuracy: <0.1% of flow) supplies a requested flow rate of gaseous fuel into the cylinder during the intake stroke. On the other hand, a 3-hole piezoelectric injector directly delivers pilot diesel into the cylinder with an ability to control injection timing and duration. Furthermore, the engine is provided with Kistler model-5011 charge amplifier and a sensor for measuring in-cylinder pressure at a resolution of 0.2 CAD.

The emission analyzing system comprises of various analyzers, which are connected to the engine with a sampling probe. The probe directly extracts a sample of raw emissions from the exhaust runner and delivers it to the analyzers. The measured emission types and principle of the employed analyzers are summarized in Table 2. In general, the engine and all auxiliary systems are instrumented with the engine control unit (ECU) using a hardware based on the national instrument field-programmable gate array (NI-FPGA). It allows a flexible control of engine operating parameters and high-speed data acquisition at 40 MHz.

**Table 2**  
Exhaust gas analyzers and measured emission types.

Emission type	Analyzer and measuring principle	Measuring range	Measurement uncertainty
UB-CH <sub>4</sub>	SIDOR non-dispersive infrared spectroscopy (NDIR) based analyzer (Sick AG)	0 – 3000 ppm	<25 ppm
THC	A heated-flame ionization detection (HFID) based analyzer Model VE-7 (J.U.M Engineering GmbH)	0 – 3000 ppm	<30 ppm
CO, CO <sub>2</sub>	SIDOR non-dispersive infrared spectroscopy (NDIR) based analyzer (Sick AG)	CO: 0 – 3000 ppm CO <sub>2</sub> : 0 – 30 vol.%	CO: ±3 ppm CO <sub>2</sub> : <0.05 vol. %
O <sub>2</sub>	a paramagnetic dumbbell (OXOR-P) analyzer (Sick AG)	0 – 25 vol. %	<0.05 vol. %
NO, NO <sub>2</sub> , NO <sub>x</sub>	CLD-822Sh (ECO Physics AG) analyzer based on chemiluminescence	NO <sub>x</sub> : 0 – 5000 ppm	<40 ppm

## 2.2. Test fuels

In the present study, methane is used as the main fuel, blended with either 0%, 10% or 20% ethane. The methane-ethane blend is port-fuel injected and ignited by a small diesel pilot. The detailed properties of the test fuels are tabulated in Table 3. The pilot fuel is an aromatic free and ultra-low sulfur diesel satisfying the ASTM D975 standard specification. It is mainly composed of paraffins and naphthenes without any olefin. On the other hand, the methane-ethane blends are produced by utilizing 99.9% pure gases, which are blended in such a way that three gaseous blends as, 1) pure methane (100M0E), 2) 10% v/v ethane enriched methane (90M10E), and 3) 20% v/v ethane enriched methane (80M20E) could be obtained. Key characteristics of the gaseous blends (also listed in Table 3) are calculated based on the gas composition. These include Wobbe index, methane number, and adiabatic flame temperature [26]. Flame temperature is calculated based on stoichiometric conditions. It is known that varying the gaseous fuel composition influences both adiabatic flame temperature and mixture fraction in the reaction zone. Wobbe index indicates the energy density of a gas, which may help to compare combustion energy output of two gaseous fuels. Moreover, methane number represents a resistance to the engine knock, where engine operations are usually considered safe for MN above 65–70.

**Table 3**  
Test fuel properties.

Properties	Diesel	100M0E	90M10E	80M20E
Molecular formula	C <sub>9</sub> – C <sub>18</sub>	CH <sub>4</sub>	C <sub>1</sub> – C <sub>2</sub>	C <sub>1</sub> – C <sub>2</sub>
Conc. CH <sub>4</sub> [vol. %]	–	100	90	80
[wt. %]	–	100	82.76	68.08
Conc. C <sub>2</sub> H <sub>6</sub> [vol. %]	–	0	10	20
[wt. %]	–	0	17.24	31.92
Cetane number	56.0	–	–	–
Paraffins [wt. %]	45.1	–	–	–
Naphthenes [wt. %]	54.9	–	–	–
Density [kg/m <sup>3</sup> ] @ 20 °C	810.2 (EN-ISO 12185)	0.66 <sup>1</sup>	0.76 <sup>1</sup>	0.85 <sup>1</sup>
Viscosity [mm <sup>2</sup> /s] @ 30 °C	2.66	17.61 <sup>2</sup>	16.33 <sup>2</sup>	15.14 <sup>2</sup>
Lower heating value (LHV) [MJ/kg]	42.25	50	49.58	49.23
Energy density [MJ/m <sup>3</sup> ]	34230.95	33.35	35.92	38.54
Wobbe index (WI) [MJ/m <sup>3</sup> ]	–	49.83 <sup>3</sup>	50.11 <sup>3</sup>	50.71 <sup>3</sup>
Methane number (MN)	–	100.00 <sup>4</sup>	81.00 <sup>4</sup>	75.00 <sup>4</sup>
A/F ratio (Stoich. wt.)	14.4	17.19	16.93	16.76
Carbon content [wt. %]	85.94	74.86	76.28	77.22
Hydrogen content [wt. %]	14.06	25.14	23.72	22.78
T <sub>adiabatic</sub> [K]	–	2324.5 <sup>5</sup>	2333.2 <sup>5</sup>	2340.7 <sup>5</sup>
T <sub>autoignition</sub> [°C]	200–300	537	470–540	470–540
C <sub>p</sub> /C <sub>v</sub> @ 25 °C	–	1.304	1.292	1.280

<sup>1</sup> density is calculated based on ideal gas law.<sup>2</sup> blend viscosity is calculated by considering gas composition,  $\nu_{mix} =$ 

$$\frac{\sum_{i=1}^N Y_i \nu_i \sqrt{M_i}}{\sum_{i=1}^N Y_i \sqrt{M_i}}$$

<sup>3</sup> Wobbe Index is calculated by using  $\frac{HHV}{\text{specific gravity}}$ .<sup>4</sup> Methane number is determined by using online Wartsilä MN calculator.<sup>5</sup> Adiabatic flame temperature is calculated for stoichiometric conditions.

### 2.3. Operating conditions and methodology

In this work, a mid-high load range of the test engine is selected for the experiments under constant operating conditions, as described in Table 4. The total-fuel energy (TFE) is also kept constant for all the experiments, wherein 97% of the TFE is contributed by the gaseous blend. The remaining 3% of the TFE is supplied by the pilot fuel. The gaseous fuel is injected into the cylinder by gas injectors at –355 CAD ATDC during the intake stroke, which is ignited by the pilot fuel directly injected at  $\theta_{SOI} = -7$  CAD ATDC. During the experiments, the test fuels are injected only after achieving stable operating conditions. An isentropic-compression temperature ( $T_{TDC}$ ) of 835 K, as calculated from Eq. (1), is maintained at firing TDC by adjusting charge-air temperature ( $T_{air}$ ). Additionally, a constant motored-peak pressure ( $MP_{peak}$ ) of 60 bar is achieved by feeding charge-air into the cylinder at a boost pressure ( $P_{air}$ ), simultaneously maintaining the charge-air mass flow rate ( $\dot{m}_{air}$ ) to

**Table 4**  
Operating conditions.

	Measurement	Measurement uncertainty
Engine speed ( $\omega$ ) [rpm]	950, 1500	±0.3% of measurement
Pilot injection pressure ( $P_{PF}$ ) [bar]	1500	±5 bar
Motored isentropic temperature at TDC ( $T_{TDC}$ ) [K]	835	±3.23 K
Motored peak pressure ( $MP_{peak}$ ) [bar]	60	±0.3 bar
Gaseous fuel equivalence ratio ( $\phi_{gas}$ )	0.52	±0.005
Methane substitution ratio	97%	±0.2%
Pilot ratio ( $P_R$ )	3%	±0.2%
Pilot injection timing ( $\theta_{SOI}$ )	–7 CAD ATDC	–
Total-fuel energy per cycle (TFE) [J/cycle]	3400	±15 J/cycle

a value resulting in a gas equivalence ratio ( $\phi_{gas}$ ) of 0.52. Furthermore, the cylinder head and the liner of the engine are preheated through the water jacket to 353 K as a pre-engine-run condition.

In order to record a reliable test data along with the data of averaged exhaust emissions, each test point is continuously run for 5 min after injecting test fuels. The in-cylinder pressure data is averaged over 100 successive combustion cycles for each test point, and undesired noise from raw-pressure data is filtered by employing a low-pass Butterworth filter algorithm. Based on the First Law of Thermodynamics, averaged pressure data is used to calculate the apparent heat release rate (HRR) and accumulative heat released (AccQ) for each test point using Eqs. (2) and (3), respectively [27]. In addition, gas equivalence ratio ( $\phi_{gas}$ ) of the charge is calculated using Eq. (4). The engine-out emissions are converted from ppm to g/kWh based on stoichiometry [27]. Additionally, combustion efficiency ( $\eta_{comb}$ ) and thermal efficiency ( $\eta_{th}$ ) are calculated using Eq. (5) and Eq. (6), respectively.

$$T_{TDC} = T_{air} \times \left( \frac{MP_{peak}}{P_{air}} \right)^{\gamma-1/\gamma} \quad (1)$$

$$HRR = \frac{dQ}{d\theta} = \frac{\gamma}{\gamma-1} P \frac{dV}{d\theta} + \frac{1}{\gamma-1} V \frac{dP}{d\theta} \quad (2)$$

$$AccQ = \int \frac{dQ}{d\theta} d\theta \quad (3)$$

$$\phi_{gas} = \frac{(AFR_{gas})_{stoichiometric}}{\left( \frac{\dot{m}_{air}}{\dot{m}_{gas}} \right)_{actual}} \quad (4)$$

$$\eta_{comb} = \frac{CO_2}{TotalC_{input}} \times 100 \quad (5)$$

$$\eta_{th} = \frac{gIMEP \times V_{displacement}}{\eta_{comb} \times TFE} \times 100 \quad (6)$$

### 2.4. Test matrix

As the main objective of the present work is to investigate the influence of ethane enrichment on diesel-methane DF combustion, three methane-ethane blends of 0–20% ethane concentration are utilized for the comparison. The test points for the present study are listed in Table 5. All experiments are conducted under constant operating conditions as tabulated in Table 3; however, in the series of experiments, two engine speeds are used to explore the effect of residence time on the combustion of varying fuel composition. Furthermore, it is worth noting that at different  $\omega$ , the operating conditions are kept constant by adjusting  $T_{air}$  and  $P_{air}$  in order to achieve constant  $T_{TDC}$  and  $MP_{peak}$ , while maintaining same total-fuel energy and charge air per cycle.

### 2.5. DF combustion interpretation

In general, DF combustion progresses with three overlapped combustion stages as a result of complex physical and chemical interactions between two fuels. These stages provide critical knowledge and an insight about combustion mechanisms, which deepens the basic reasoning for DF combustion process and its emission characteristics. Fig. 2 shows an example of two typical DF HRR profiles investigated in this study (as will be discussed in Section 3), which are marked with the combustion stages as  $\theta_1$ ,  $\theta_2$ , and  $\theta_3 = \theta_{3a} + \theta_{3b}$  along with  $\theta_{90}$ . Here  $\theta_1$ ,  $\theta_2$  and  $\theta_3$  denote the start of the first (I)-, second (II)-, and third (III)- stage combustion, respectively. The combustion stages are characterized as: I) combustion of pilot fuel and entrained gaseous fuel, II) burning of the gaseous fuel in the vicinity of the ignited pilot fuel, and III) combustion of the remaining premixed gaseous fuel. These stages are identified from HRR by using the second derivative analysis as presented in our previous

**Table 5**  
Experimental test points.

Main Fuel Type	$\omega$ [rev/min]	$\dot{m}_{PF}$ [mg/cycle]	$\dot{m}_{CH_4}$ [mg/cycle]	TFE [J/cycle]	gIMEP [bar]	$\eta_{comb}$ [%]	$\eta_{th}$ [%]
100M0E	950	2.3	65.7	3428.9	12.02	97.73	50.33
	1500	2.3	64.7	3335.5	11.18	91.74	51.27
90M10E	950	2.3	67.0	3428.2	11.91	98.06	49.71
	1500	2.3	66.4	3395.8	12.34	95.82	53.21
80M20E	950	2.3	66.7	3386.7	11.80	98.2	49.78
	1500	2.3	67.5	3429.3	12.66	96.7	53.57

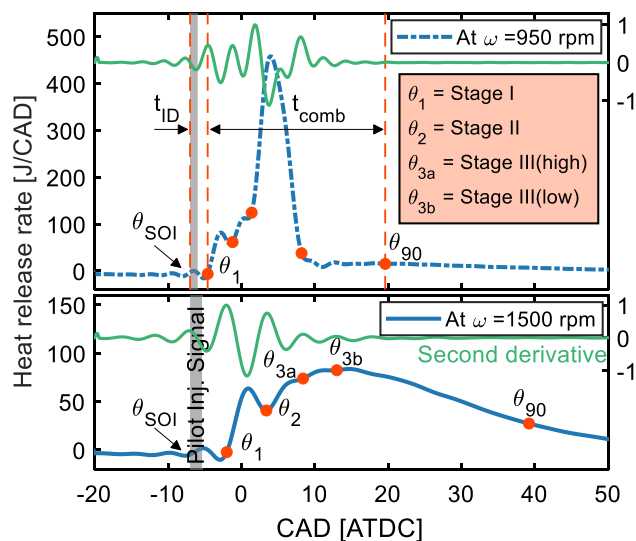


**Fig. 2.** An example showing the three overlapping DF combustion stages determined from typical HRR profiles investigated in this study. The stages are identified by the second derivation of HRR analysis. It is interesting to note that the profiles of the HRR curves tend to change from multi-peaks (M-shaped) to quasi-single peak with decreasing  $\omega$  from 1500 rpm to 950 rpm.

work [28]. On the other hand,  $\theta_{90}$  is determined as a CAD where 90% of the total heat (AccQ) is released. In this work, experimental ignition-delay time ( $t_{ID}$ ) is defined as a time interval between  $\theta_{SOI}$  and  $\theta_1$ , whereas combustion duration ( $t_{comb}$ ) is defined as a time interval between  $\theta_1$  and  $\theta_{90}$ , as shown in Fig. 2.

### 3. Numerical simulations and methods

In this study, we perform zero-dimensional (0D) and one-dimensional (1D) numerical simulations phenomenologically under engine relevant conditions (according to Table 4) using Cantera [29]. The calculated ignition-delay time ( $t_{ID}$ ) is defined as the time instance when 0D-reactor temperature versus time reaches its maximum gradient, which is consistent with the maximum gradient of OH mass fraction versus time. Furthermore, a theoretical analysis approach, called  $\beta$ -curve, recently developed by Karimkashi et al. [30] is employed to determine the influence of ethane enrichment on the combustion propagation mode. Three gaseous blends as listed in Table 3 are used for comparison, while n-dodecane is considered as the pilot-diesel surrogate. Detailed information about the utilized chemical-kinetic mechanism and its validation are provided in Appendix A.

#### 3.1. $\beta$ -curve methodology

In engine experiments, identification of the exact combustion mode is challenging. For this purpose, the theoretical  $\beta$ -curve analysis is used herein. This method helps to distinguish the prevalence of deflagration (flame propagation) against spontaneous auto-ignition in DF engines. It considers different levels of mixture stratification, i.e. reactivity

stratification, relevant to DF engines with two parameters  $Y'$  and  $\lambda$  of a presumed sinusoidal distribution. The amplitude ( $Y'$ ) characterizes the level of stratification of diesel within the premixed charge, and the wavelength ( $\lambda$ ) represents a spatial dimension or space of the local mixture.  $\beta = S_L/S_{ign}$ , is defined as the ratio of laminar flame speed ( $S_L$ ) to ignition-wave speed ( $S_{ign}$ , indicated by the inverse of ignition-delay time gradient in the system according to [31]). An illustration of  $\beta$ -curve analysis is presented in Fig. 3.

According to the figure, the curved black line represents a border line ( $\beta = 1$ ) separating two combustion mode regions i.e. deflagration and spontaneous auto-ignition. It shows that spontaneous auto-ignition occurs below the border line ( $\beta = 1$ ) while the deflagration mode may be observed above the line. If ignition-wave speed is higher than the laminar flame speed ( $\beta < 1$ ), the mode of combustion propagation is spontaneous auto-ignition (volumetric). On the contrary,  $\beta > 1$  is interpreted as deflagration (flame propagation) mode. For example, the more the  $\beta = 1$  curve is shifted to the deflagration region (expanding  $\beta < 1$  region), the more probable is the spontaneous auto-ignition mode of combustion in the selected range of  $Y'$  and  $\lambda$ .

We note that here,  $\lambda_{diffusion} = 2\pi\sqrt{\nu\tau}$ , is defined similar to the definition in [30], which is used for normalizing  $\lambda$ .  $\tau$  is simply the calculated  $t_{ID}$  from 0D simulations and  $\nu$  is the kinematic viscosity. Also,  $Y'$  is normalized by the maximum stratification amplitude considered and it is denoted as  $Y'_{norm}$  in the analysis. More information about the  $\beta$ -curve calculations and its derivation is provided in Section 4.2 and Appendix B, respectively.

### 4. Results and discussions

In this section, we report experimental results of three gaseous blends to demonstrate the influence of ethane enrichment on DF combustion and emission characteristics. Additionally, we present 0D and 1D numerical analysis to complement the comparison and determine the effect of ethane on combustion propagation mode by using  $\beta$ -curve

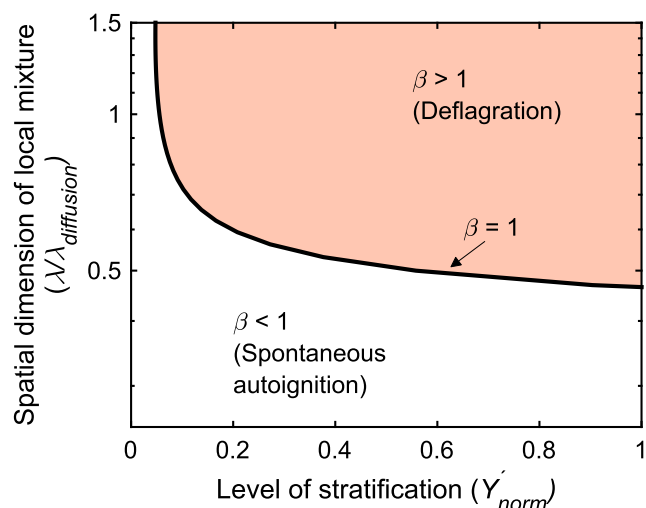


**Fig. 3.** Illustration of  $\beta$ -curve analysis.

analysis (Section 3.1). Furthermore, in the following, to aid with interpretation of the combustion process, combustion stages are distinguished from similar HRR profiles according to Fig. 2 (Section 2.5).

4.1. Experimental results

4.1.1. Influence of ethane enrichment on combustion characteristics

Figs. 4–7 show a comparison and present combustion characteristics of all three gaseous blends at two engine speeds. We begin the analysis by discussing ignition-delay time and combustion duration. These are two of the important parameters to characterize and comprehend a combustion process. Ignition-delay time ( $t_{ID}$ ) indicates the ignitability and reactivity of a fuel–air mixture, whereas combustion duration ( $t_{comb}$ ) represents the combustion rates and time taken to complete a combustion process. Fig. 5 shows the experimental results of  $t_{ID}$  and  $t_{comb}$ . It is observed that ethane enrichment has less significant effect on pilot diesel in reducing ignition-delay time at both engine speeds, although it enhances the ignitability of pure methane. In addition, increasing ethane concentration from 10% (90M10E) to 20% (80M20E) does not reduce ignition-delay time any further. The similar results have also been reported in our previous experimental study by Ahmad et al. [24]. This implies that the changes in ignitability and reactivity of pure methane due to ethane addition during pre-ignition processes are not viable to improve overall DF combustion phasing. However, we consider this

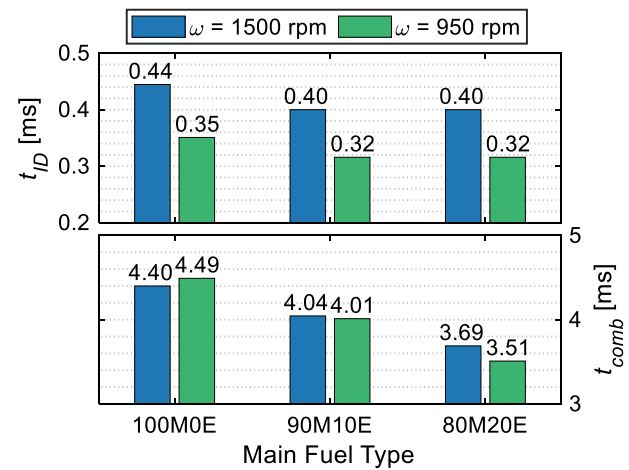
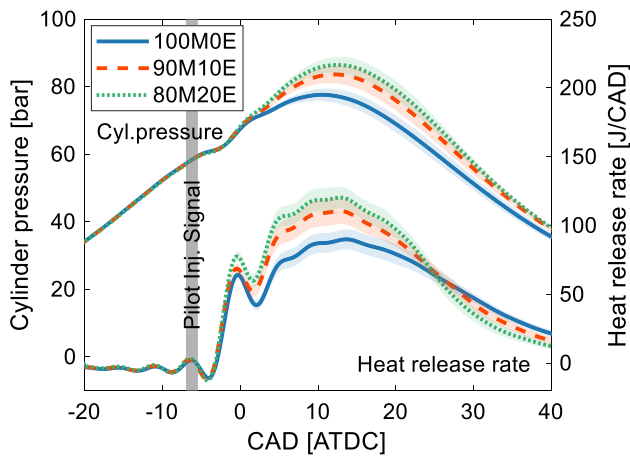
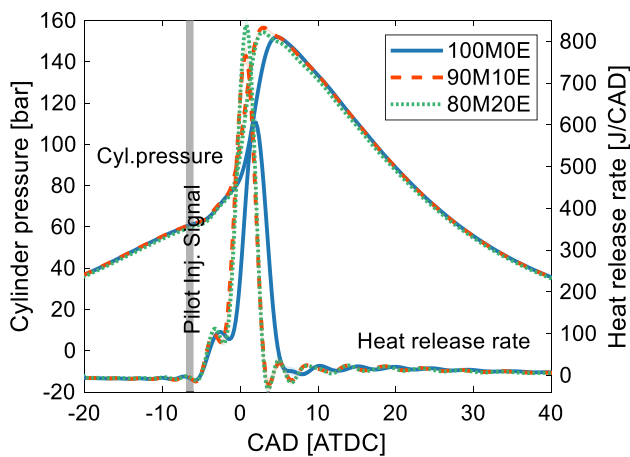


Fig. 5. Experimental  $t_{ID}$  and  $t_{comb}$  results for all three gaseous fuel blends at two different engine speeds under constant operating conditions.



(a)  $\omega=1500$  rpm and  $P_{PF}=1500$  bar



(b)  $\omega=950$  rpm and  $P_{PF}=1500$  bar

Fig. 4. Averaged experimental cylinder pressure and HRR traces with standard deviation for all three gaseous blends at two engine speeds. The operating conditions at both engine speeds are kept constant according to Table 4.

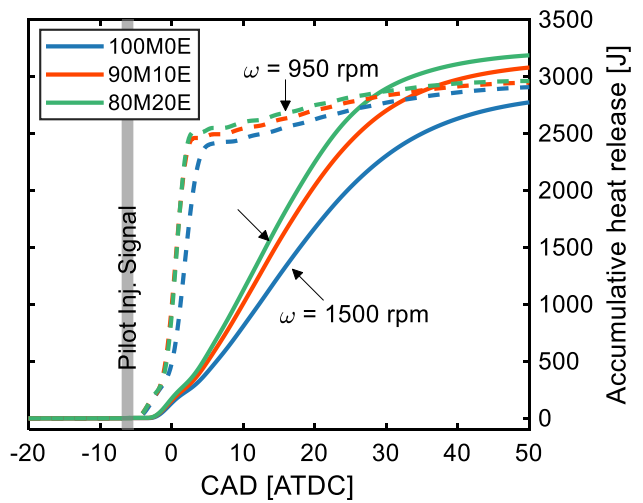


Fig. 6. Experimental AccQ traces for three gaseous blends at two different engine speeds under constant operating conditions.

deduction as a standing hypothesis for the later 0D and 1D analysis.

On the other hand, compared to pure methane (100M0E), ethane enriched gaseous blends (90M10E and 80M20E) substantially reduce combustion duration at both engine speeds, as shown in Fig. 5. This establishes that ethane addition to pure methane considerably influences the combustion processes after the start of combustion. This can also be examined from the in-cylinder pressure traces and HRR, presented in Fig. 4. At both engine speeds, 90M10E and 80M20E produce a higher peak combustion pressure and HRR than 100M0E. An increase in the concentration of ethane from 0% to 20% in a blend monotonically increases peak combustion pressure and peak HRR. It is worth noticing that after the start of combustion during Stage I, peak HRR increases with an increase in ethane concentration despite a probable decrease in  $t_{ID}$ . Since  $t_{ID}$  has a direct influence on the heat release during Stage I, it is usually understood that a longer  $t_{ID}$  leads to a higher peak HRR compared to a shorter  $t_{ID}$ . For a longer  $t_{ID}$ , a pilot fuel has a longer time available to entrain greater amount of premixed gaseous fuel and burn it during Stage I [28]. However, here the contrary trend is due to varying ethane concentration from 0% to 20%, prompting higher energy density and Wobbe index for 90M10E and 80M20E than 100M0E (see Table 3). After the start of combustion, this high-density energy release leads to increased mixture reactivity by yielding locally high temperatures. Correspondingly, ethane enriched gaseous blends (90M10E and

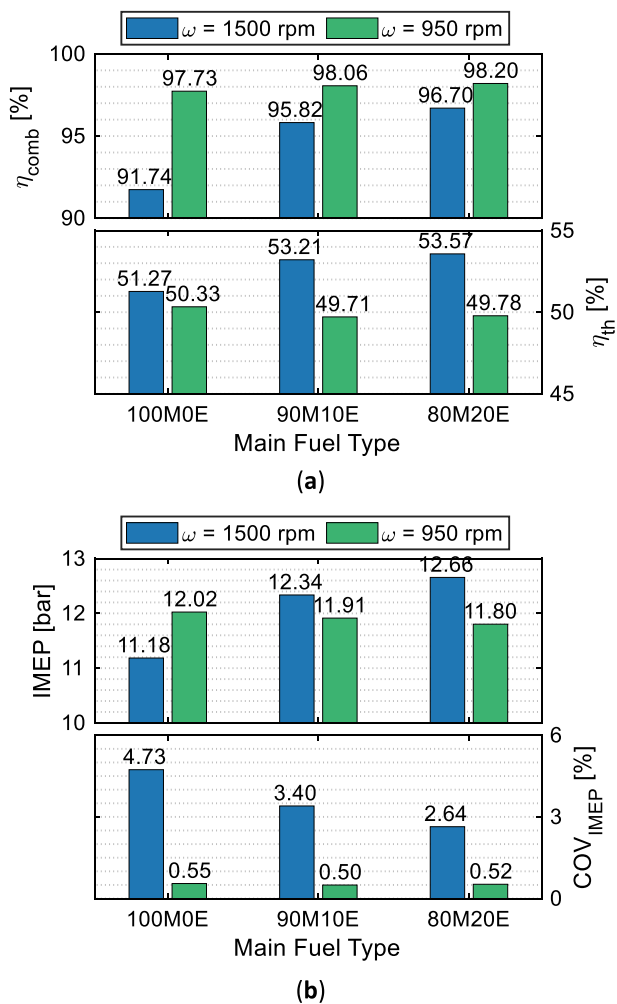


Fig. 7. (a)  $\eta_{comb}$  and  $\eta_{th}$  results; (b) IMEP and COV<sub>IMEP</sub> results for all three gaseous blends at two different engine speeds under constant operating conditions.

80M20E) tend to burn with higher adiabatic flame temperatures than pure methane (100M0E) [32].

As pointed out, the differences in peak HRR during Stage I for all three gaseous blends are rather clear. However, these differences become further distinctive when DF combustion progresses during Stages II and III, wherein combustion is principally dominated by pre-mixed gaseous fuel (Section 2.5). Therefore, it is plausible to remark that  $t_{comb}$  is reduced due to an increase in the reactivity of the gaseous fuel induced by local high-density heat release (which is seemingly insignificant during pre-ignition processes). Based on this, it is suggested that ethane addition to pure methane may increase the mixture reactivity to such an extent that the dominant combustion mode for premixed gaseous fuel during Stage II and III can possibly transit from flame propagation (deflagration) to spontaneous auto-ignition or simultaneously both. We consider this deduction yet another standing hypothesis for the later 0D and 1D analysis.

In general, a change in engine speed directly affects overall combustion performance. For instance, at a lower engine speed, time per CAD ( $t_{CAD}$ )<sup>1</sup> increases and as a result greater amount of fuel burns per CAD. It can be clearly seen from Fig. 4 that at 950 rpm, DF combustion yields substantially higher combustion rates. Besides, the HRR profiles

<sup>1</sup> At  $\omega=1500$  rpm,  $t_{CAD} = 0.111$  ms, whereas at  $\omega=950$  rpm,  $t_{CAD} = 0.17544$  ms.

are slightly different from the profile illustrated at 950 rpm in Fig. 2. This is due to an overlap of  $\theta_2$  and  $\theta_{3a}$ , which can be attributed to almost complete depletion of the pilot fuel during Stage I.

Likewise, it is also observed in Fig. 5 that  $t_{ID}$  and  $t_{comb}$  decrease at 950 rpm compared to 1500 rpm. The decrease in  $t_{ID}$  is due to the reduced level of in-cylinder turbulence and longer residence time [33], while  $t_{comb}$  shortens due to rapid combustion. It should be noted that for pure methane (100M0E),  $t_{comb}$  is a bit longer at 950 rpm compared to that at 1500 rpm. This increase in  $t_{comb}$  is due to the slow heat release during low-intensity regime of Stage III between  $\theta_{3b}$  and  $\theta_{90}$ . During this tail combustion close to  $\theta_{90}$ , dilution or flame quenching yields slow HRR, which causes the overall  $t_{comb}$  to extend at 950 rpm. Since the introduction of ethane into pure methane improves reactivity,  $t_{comb}$  reduces for ethane enriched gaseous fuels (90M10E and 80M20E) at 950 rpm more than at 1500 rpm. This effect becomes even more distinctive when ethane concentration is increased from 10% to 20%. However, it is interesting to note that  $t_{comb}$  expressed in units of time (ms) is comparable for both engine speeds.

Figs. 6–7 illustrate the combustion performance trends for all gaseous fuels at two engine speeds. According to the figures, ethane enrichment leads to burn greater amount of fuel and yields monotonically higher AccQ and  $\eta_{comb}$  for both engine speeds. Additionally, it reduces coefficient of variability of IMEP [24,34]. However, at 950 rpm, the effect of ethane enrichment has lower significance. It is surprising to note that compared to 1500 rpm, AccQ,  $\eta_{th}$  and IMEP decrease at 950 rpm especially for ethane enriched gaseous fuels (90M10E and 80M20E). This seems to be due to the early combustion phasing and particularly higher heat losses. As it can be seen from Fig. 6, around 3 CAD ATDC,  $\sim 85\%$  ( $\sim 60$  for 100M0E) of the total heat is released at 950 rpm while at 1500 rpm for an equivalent time scale only  $\sim 35\%$  of total heat is released. This indicates that dilution during tail combustion is more significant for 950 rpm cases (90M10E and 80M20E), which consequently produces lower AccQ than that at 1500 rpm. However,  $\eta_{comb}$  increases for all gaseous blends at 950 rpm because emission-based calculations represent gross fuel-energy release including heat losses. The  $\eta_{comb}$  trends can also be examined from emission characteristics.

#### 4.1.2. Influence of ethane enrichment on emission characteristics

Next, we look at the emission trends of the methane-ethane blends. Fig. 8 represents the influence of ethane enrichment on emission characteristics. It is observed that at both engine speeds, varying ethane concentration from 0% to 20% in a blend significantly reduces unburned CH<sub>4</sub>, THC and CO emissions at an expense of producing higher CO<sub>2</sub> and NO<sub>x</sub>. Adding ethane into pure methane reduces unburned CH<sub>4</sub> emissions not only because of replacing methane with ethane but also due to the increased mixture reactivity, as explained earlier. This increased mixture reactivity leads to burning more fuel and causes reduced THC at both engine speeds. Additionally, CO emissions decrease due to the locally high temperature combustion and relatively richer mixtures, as carbon content increases in a blend with an increase in ethane enrichment. Furthermore, it is observed that at 950 rpm owing to higher reaction rates, the emission levels are reduced compared to 1500 rpm. However, the effect of ethane enrichment at 950 rpm is not as significant as at 1500 rpm.

In a combustion process, NO<sub>x</sub> emissions usually increase because of high in-cylinder temperature and longer residence time. Therefore, in Fig. 8, NO<sub>x</sub> emissions are observed to increase with an increase in ethane enrichment, as 90M10E and 80M20E burn with higher adiabatic flame temperatures. However, the substantially higher NO<sub>x</sub> levels at 950 rpm are due to the longer residence time per CAD and higher combustion rates. In the same manner, CO<sub>2</sub> emission increases with ethane addition and yields correspondingly higher  $\eta_{comb}$ , as shown in Fig. 7(a).

In summary, we observed here (Section 4.1) that increasing ethane concentration in a blend from 0% to 20% monotonically increases  $\eta_{comb}$ ,  $\eta_{th}$  and IMEP at engine speed of 1500 rpm. However, due to higher heat losses at 950 rpm, ethane enrichment reduces  $\eta_{th}$  and IMEP. Also,

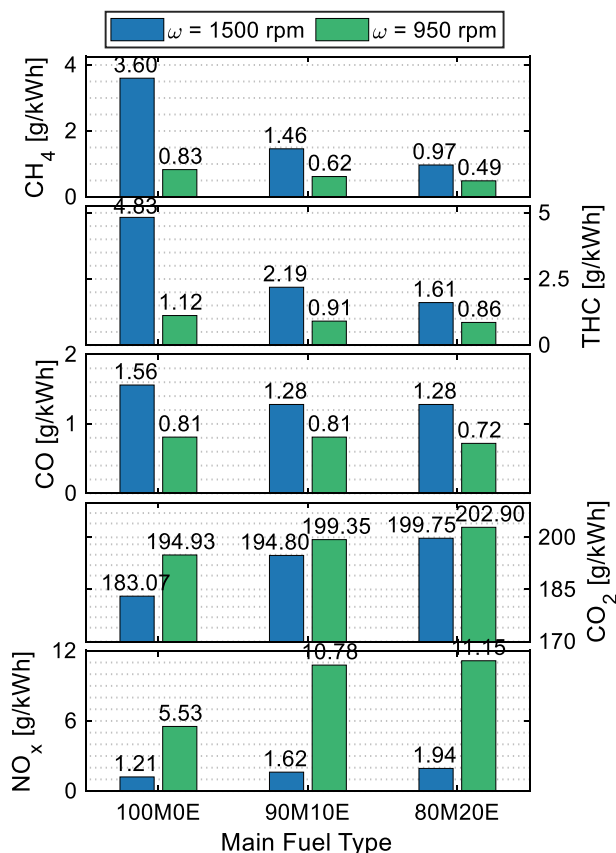


Fig. 8. Experimental exhaust emission data for all three gaseous blends at two different engine speeds under constant operating conditions.

90M10E and 80M20E could not yield higher AccQ,  $\eta_{th}$  and IMEP than that at 1500 rpm. On the other hand, at 950 rpm 90M10E and 80M20E produce substantially higher NO<sub>x</sub> than 100M0E with slightly improved combustion.

#### 4.2. Numerical and theoretical results

To further elaborate the influence of ethane enrichment on experimental results, namely 1)  $t_{ID}$  and 2)  $t_{comb}$ , zero-dimensional (0D) and one-dimensional (1D) numerical-simulation results are presented in this section under engine relevant conditions (Table 4). Here  $t_{ID}$  is calculated in 0D homogeneous reactor simulations using a mixing line concept [35]. Laminar flame speed ( $S_L$ ) is calculated from 1D planar adiabatic flame calculations as a qualitative measure of  $t_{comb}$ . In addition,  $\beta$ -curve analysis is employed to determine the influence of ethane enrichment on the combustion propagation mode, which is also directly relevant to  $t_{comb}$ .

##### 4.2.1. Ignition-delay time

Fig. 9 shows 0D simulation results for  $t_{ID}$  at the pressure  $MP_{peak} = 60$  bar and the temperature range investigated in engine experiments. According to the figure, a similar trend of  $t_{ID}$  is observed as illustrated by experiments, i.e. ethane enrichment increases ignitability and reduces  $t_{ID}$ . However, here  $t_{ID}$  values are significantly larger than that listed for experiments in Fig. 5. This is due to the fact that in engines, diesel and premixed gaseous fuel are not homogeneously mixed, and ignition typically initiates at the most reactive mixture fraction within the stratified charge. Therefore, to account for the mixture stratification, a mixing line concept is adopted for the 0D simulations.

Mixing line concept helps to interpret 0D homogenous reactor calculations for CI engines. In this concept, two streams of 1) a cold diesel

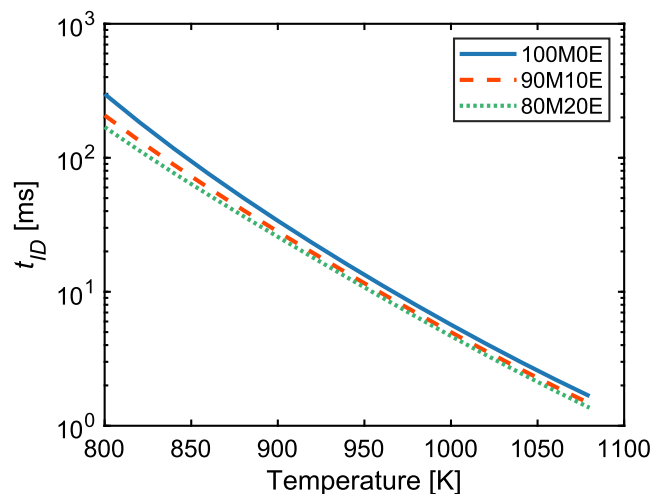


Fig. 9. Calculated  $t_{ID}$  results given by 0D numerical simulations in homogeneous reactor at a range of temperature.

surrogate and 2) a hot premixed charge are envisioned to mix inside a 0D reactor at various relevant mixture fractions prior to simulations. Mixture fraction ( $\xi$ ) is defined according to Bilger et al. [36] as the mixing extent of the diesel surrogate into a constant quantity of premixed gaseous fuel, e.g.  $\xi = 1$  denotes pure diesel surrogate and  $\xi = 0$  indicates the pure premixed gaseous fuel. In other words,  $\xi$  is equivalent to the pilot ratio of diesel surrogate in the charge. Thus, to imitate mixture stratification during pre-ignition processes,  $t_{ID}$  is calculated at a wide range of  $\xi$  values (between 0 and 1), considering the mixture temperature and other thermal differences between diesel surrogate and the gaseous fuel. More information can be found in [35].

Fig. 10 displays calculated  $t_{ID}$  values based on the mixing line concept. Here, the most reactive mixture fraction ( $\xi_{MR}$ ) is defined as the mixture fraction at which  $t_{ID}$  is the shortest among each considered mixture ( $\sim \xi_{MR} = 0.05$ ). Moreover, it should be noted that in engine experiments, ignition typically starts at a mixture fraction leaner than  $\xi_{MR}$  and richer than the stoichiometric mixture fraction ( $\xi_{St} = 0.031$ ), indicated by the region of 1st ignition. Accordingly, it is observed from the figure that the differences in  $t_{ID}$  among all three gaseous blends for the whole range of  $\xi$  including  $\xi_{MR}$  are very small, meaning that the influence of ethane enrichment during pre-ignition is insignificant, as consistent with the experimental results. This explicitly proves our

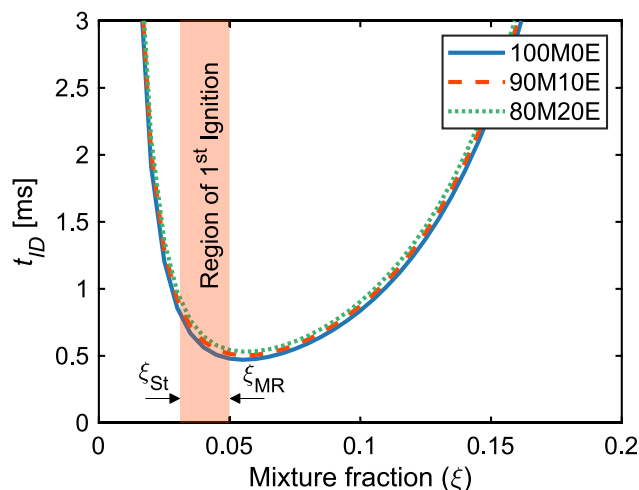


Fig. 10. Calculated  $t_{ID}$  results for all three gaseous blends given by 0D homogeneous reactor simulations using mixing line concept for stratified mixture fractions within the engine.

hypothesis that the changes in ignitability and the reactivity of pure methane due to ethane enrichment during pre-ignition processes are not viable to improve overall DF combustion phasing.

#### 4.2.2. Combustion duration

Since premixed gaseous fuel shares 97% of the total-fuel energy, it is suggested that  $t_{comb}$  predominantly depends on the burning ability of the premixed gaseous fuel. Fig. 11 represents calculated  $t_{ID}$ , in a boarder range of mixture fraction values compared to Fig. 10, to underline the ignitability and reactivity of pure premixed gaseous fuel ( $\xi = 0$ ). It is observed that although all three gaseous blends have similar  $t_{ID}$  values at their corresponding  $\xi_{MR}$  (Fig. 10), there is a significant difference in reactivity of pure premixed gaseous fuels at  $\xi = 0$ . This implies that after the start of combustion, gaseous fuel has the potential to burn faster with ethane enrichment, i.e. shorter  $t_{comb}$ , which is consistent with experimental finding. However, to quantify this, laminar flame speed ( $S_L$ ) is calculated for all gaseous blends at  $\xi = 0$  and  $\xi_{MR}$  under engine relevant operating conditions i.e.  $MP_{peak} = 60$  bar and  $T_{TDC} = 835$  K. It can be seen in Fig. 12 that adding ethane into pure methane increases  $S_L$  for both  $\xi = 0$  and  $\xi_{MR}$  cases, which is consistent with the shorter  $t_{comb}$ . However, these differences in  $S_L$  are rather small, suggesting that increased  $S_L$  with ethane enrichment could not possibly be the only factor in improving diesel-methane DF combustion. Therefore, in the following, combustion propagation mode analysis is carried out to shed more light on the reason of shorter  $t_{comb}$  and higher  $\eta_{comb}$ .

#### 4.2.3. Combustion mode analysis

In order to analyze the influence of ethane enrichment on combustion propagation modes,  $\beta$ -curve analysis is adopted, as explained in Section 3.1 and Appendix B. Fig. 13 represents theoretical  $\beta$ -curves for all three gaseous blends. Here,  $\beta=1$  curves are compared for the shift into either of two probability regions with an ethane enrichment. It is observed that adding ethane into pure methane shifts  $\beta = 1$  curves upward such that the spontaneous auto-ignition region expands compared to the deflagration region for the same level of stratification. Here, the expansion in spontaneous auto-ignition region is noted to be due to a decrease in  $\alpha$  ( $\alpha$ -lines in Fig. 11,  $\alpha_1 > \alpha_2 > \alpha_3$ ), which is a linear approximation for variation of  $t_{ID}$  with respect to  $\xi$ , as explained in Appendix B. This implies that ethane enrichment leads the DF combustion process to approach HCCI conditions. In other words, compared to pure methane, ethane-enriched gaseous blend would have more tendency towards ignition spots during combustion than flame propagation (deflagration),

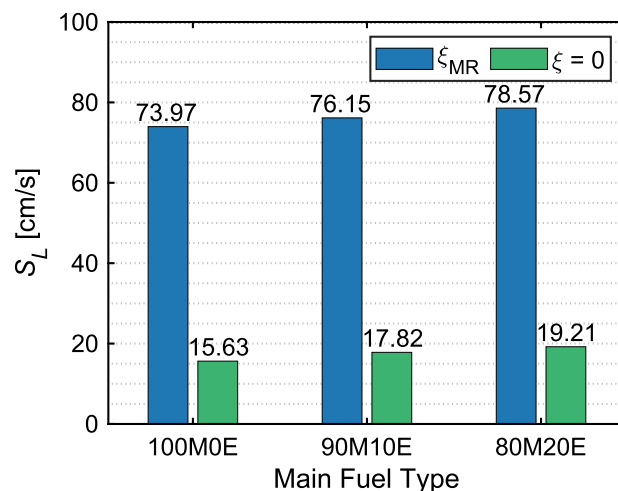


Fig. 12. Calculated  $S_L$  for all three gaseous blends at  $\xi = 0$  and  $\xi_{MR} = 0.05$  under engine relevant conditions of 60 bar and 835 K; using Polimi reduced mechanism.

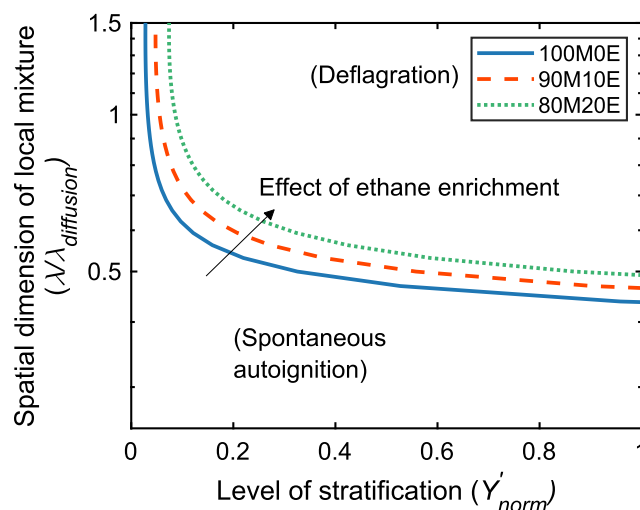


Fig. 13.  $\beta = 1$  curves of all three gaseous fuels showing the influence of ethane enrichment on combustion propagation mode.

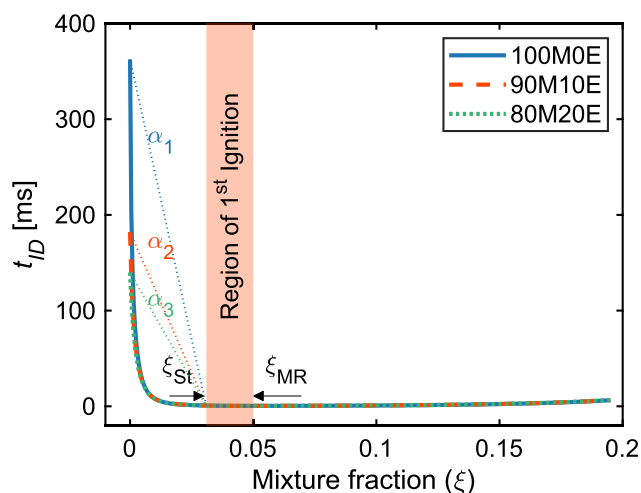


Fig. 11. Calculated  $t_{ID}$  results for all three gaseous blends given by 0D homogeneous reactor simulations using mixing line concept for various mixture fractions within the engine (signifying ignition delay for  $\xi = 0$ ). For the interpretation of dotted  $\alpha$ -lines, see Appendix B.

as also hypothesized from experimental results. This would lead to burn greater amount of fuel and shorter  $t_{comb}$ .

Overall, numerical simulations and the provided theoretical analysis are in line with experimental results, which proves our hypotheses regarding  $t_{ID}$  and combustion mode in relevance to  $t_{comb}$ . It is demonstrated that ethane enrichment does not significantly influence ignitability of the gaseous fuel during pre-ignition processes. In addition, variations in  $S_L$  are small. However, the reactivity of the premixed gaseous fuel considerably increases after the start of combustion with ethane enrichment. Consequently, this high reactivity makes spontaneous auto-ignition more probable compared to flame propagation as confirmed by the  $\beta$ -curve analysis. Since, spontaneous auto-ignition is faster to consume fuel than that of deflagration, shorter  $t_{comb}$  and higher  $\eta_{comb}$  is observed for the cases with more ethane enrichment.

## 5. Conclusions

In this work, the influence of ethane enrichment on lean ( $\phi_{gas} = 0.52$ ) diesel-methane DF combustion is studied experimentally in a single-cylinder DF engine. Experiments are performed for two engine speeds by keeping the TFE and engine operating conditions constant. In

addition, to complement the experimental results phenomenologically, calculated  $t_{ID}$  and  $S_L$  results are presented from 0D and 1D numerical simulations using Cantera. Also, theoretical  $\beta$ -curve analysis is used to determine the mode of combustion. Three gaseous blends of varying ethane concentration of 0%, 10% and 20% are adopted for comparison. In these test cases, 97% (TFE based) of the gaseous blend is ignited by a small 3% (TFE based) pilot. The main findings of the present work are concluded in the followings.

- Both experiments and numerical simulations indicate that;
  - Ethane enrichment has a less significant reducing effect on pilot-diesel ignition ( $t_{ID}$ ), which is void of changing DF combustion phasing.
  - Adding ethane into pure methane reduces combustion duration significantly due to the higher laminar flame speed ( $S_L$ ) and increased mixture reactivity induced by higher-density heat release after the start of combustion.
  - Increased ignitability and mixture reactivity of the premixed gaseous fuel due to ethane addition may transform the mode of combustion from flame propagation (deflagration) to spontaneous auto-ignition or simultaneously both. In other words, combustion process could approach HCCI conditions. This may particularly lead to reduced combustion duration with considerable higher combustion efficiency.
- Ethane enrichment increases DF combustion performance owing to combustion processes after the start of combustion. Increasing ethane content into pure methane yields monotonically higher peak cylinder pressure, peak HRR, AccQ, IMEP, thermal and combustion efficiency.
- At lower engine speeds, DF combustion improves due to lower in-cylinder turbulence and longer residence time per CAD, producing higher combustion efficiency. However, the significance of ethane enrichment is lower at 950 rpm compared to 1500 rpm especially in terms of IMEP and thermal efficiency due to higher heat losses.
- Adding ethane into pure methane, considerably reduces engine-out emission of unburned-CH<sub>4</sub>, THC and CO at an expense of higher NO<sub>x</sub> and CO<sub>2</sub>. Unburned-CH<sub>4</sub> emissions are reducing not only due to replacing methane with ethane but also due to higher combustion efficiency.
- NO<sub>x</sub> emissions increase with ethane enrichment because it increases the adiabatic flame temperature of the mixture. In addition, especially at 950 rpm, ethane enriched gaseous blends (90M10E and 80M20E) yield substantially higher NO<sub>x</sub> emissions due to higher combustion rate and bulk in-cylinder temperature.
- Under lean conditions, ethane enrichment into methane helps significantly in reducing the cyclic variations (COV<sub>IMEP</sub>). The effect is more evident at higher engine speeds.

The overall observations reveal that ethane enrichment can potentially improve diesel-methane combustion under lean conditions and impact environment positively. With only 10% ethane addition, ~59% unburned-CH<sub>4</sub> emissions are reduced with a gain of ~ 4% in thermal efficiency and ~ 4.5% in combustion efficiency at 1500 rpm. On the other hand, the significance of ethane enrichment reduces at lower engine speeds.

#### CRediT authorship contribution statement

**Zeeshan Ahmad:** Investigation, Validation, Methodology, Data

#### Appendix A. . Chemical mechanism validations

There are several limitations in validation of chemical mechanisms under engine relevant conditions, especially for blends of two or more fuels with limited experimental data on  $t_{ID}$  and  $S_L$ . In the current numerical simulations, Polimi reduced mechanism developed by Frassoldati et al. [37] is

**Table A1**

Experimental methane-ethane blends by Petersen et al. [39] used for the validation of Polimi reduced mechanism in Cantera.

	X (mole fractions)	Pressure (atm)
Mixture 1: 90% methane/ 10% ethane	'CH4': 0.0419, 'C2H6': 0.0047, 'O2': 0.2003, 'N2': 0.7531	22.4
Mixture 2: 70% methane/ 30% ethane	'CH4': 0.0288, 'C2H6': 0.0123, 'O2': 0.2015, 'N2': 0.7574	22

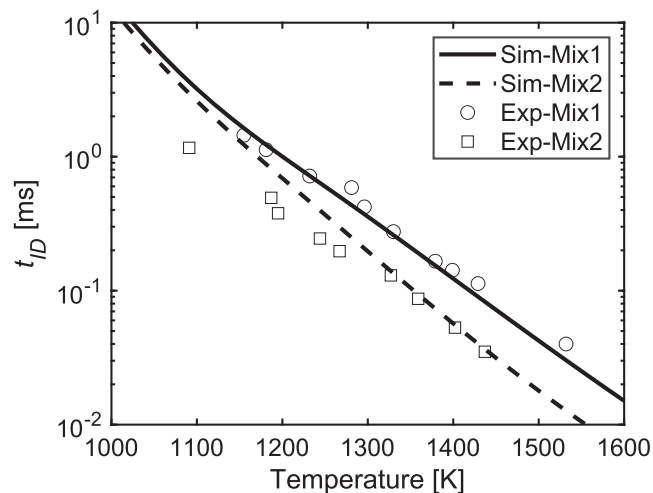


**Fig. A1.** Calculated  $t_{ID}$  results using Polimi reduced mechanism against initial temperature of methane-ethane mixtures listed in Table A1 compared to the experiments in Ref. [39].

curation, Formal analysis, Visualization, Writing - original draft, Writing - review & editing. **Ossi Kaario:** Conceptualization, Resources, Writing - review & editing, Supervision. **Shervin Karimkashi:** Software, Data curation, Formal analysis, Methodology, Writing - review & editing. **Cheng Qiang:** Investigation. **Ville Vuorinen:** Supervision, Funding acquisition. **Martti Larmi:** Supervision, Funding acquisition.

#### Declaration of Competing Interest

The authors declare that they have no known competing financial interests or personal relationships that could have appeared to influence the work reported in this paper.

#### Acknowledgments

This study has been financially supported by Academy of Finland projects (grant no. 13297248, 318024 and 332784) and Fortum-Neste Foundation (grant no. 20190102). The project has also received funding from the European Union's Horizon 2020 research and innovation program under grant agreement no 634135. The financial assistances are gratefully acknowledged.

utilized for n-dodecane combustion. For brevity, we rely on previous validations of Polimi reduced for single-fuel n-dodecane in [37], and for dual-fuel n-dodecane/methane in [38]. However, here we provide validations for mixtures of methane-ethane considering available data in the literature. In this respect, experimental data by Petersen et al. [39] for two different blends of methane-ethane at high pressure conditions, reported in Table A1, are used against  $t_{ID}$  calculations by Polimi reduced mechanism in Cantera. Fig. A1 compares the experimental data against our OD homogeneous reactor calculations using Polimi reduced for a wide range of temperature variations between 1000 K and 1600 K. This result implies that Polimi reduced mechanism calculations are reliably comparable with experimental data for blends of methane-ethane. We note that as there is no  $t_{ID}$  experimental data for n-dodecane-ethane or n-dodecane-ethane-methane, we rely on the provided validations for using Polimi reduced mechanism in this study. It is also noteworthy that there is no chemical mechanism developed for dual-fuel or tri-fuel combustion of n-dodecane with methane-ethane. Thereby, we find Polimi reduced mechanism a good choice for this tri-fuel problem according to justifications in the recent tri-fuel n-dodecane-methane-hydrogen study by Karimkashi et al. [40].

## Appendix B. $\beta$ -curve methodology

In  $\beta$ -curve analysis, a transient diffusion–reaction problem is solved to consider reactivity versus diffusion prevalence under engine relevant conditions. This theoretical analysis is validated using numerical simulations in [30] and it is inserted into the  $\beta$  definition, which provides the following equation.

$$Y' = \frac{\beta \lambda \exp(4\pi^2 \nu_{eff} \tau / \lambda^2)}{C_\beta S_L \alpha 2\pi} \quad (B1)$$

In Eq. (B1),  $\beta = 1$  specifies the borderline between the two modes of combustion (deflagration versus spontaneous auto-ignition),  $\nu_{eff}$  is effective mass diffusivity which also includes effects of turbulent convection into account,  $\tau$  is a timescale of order  $t_{ID}$  at  $\xi_{MR}$ ,  $C_\beta$  is a constant of order unity, and  $\alpha$  ( $\alpha$ -lines in Fig. 11) denotes a linear approximation for variation of  $t_{ID}$  with respect to  $\xi$ .

Here  $\beta$ -curve ( $\beta = 1$ ) is plotted within a specific range of ( $Y'$ ,  $\lambda$ ) and the shift of  $\beta$ -curve with ethane enrichment is studied. We estimate  $\alpha$  as the linear slope of  $t_{ID}$  versus mixture fraction i.e.  $d(t_{ID})/d(\xi)$  according to Fig. 11 when  $0 < \xi < \xi_{MR}$ . Moreover, we assume that  $\nu_{eff}$  does not vary between different engine tests as all tested mixtures have similar diffusivity and also, turbulence parameters are statically similar between our different engine tests. Values of  $t_{ID}$  and  $S_L$  at  $\xi_{MR}$  are utilized according to Fig. 10 and Fig. 12, respectively.

With relevance to the theoretical analysis provided in Fig. 13 we note that here,  $t_{ID}$  and  $S_L$  at  $\xi_{MR}$  do not change significantly between the three gaseous blends according to the results. In addition,  $Y'$  and  $\lambda$  are parameters related to the stratification level, which do not change significantly in our experiments with same engine setups, which is true also for  $\nu_{eff}$ . Therefore, in Eq. (B1), the only parameter that is changing significantly is  $\alpha$ . Considering Fig. 11, with adding ethane to the mixture,  $\alpha$  decreases significantly,  $\alpha_1 > \alpha_2 > \alpha_3$ . When  $\alpha$  decreases, spontaneous propagation region expands as shown in Fig. 13.

## References

- [1] IEA. The Role of Gas in Today's Energy Transitions, IEA, Paris; 2019. <https://www.iea.org/reports/the-role-of-gas-in-todays-energy-transitions>. Accessed July 22, 2020.
- [2] Alternative fuels, European commission expert group report (studies and report), <https://ec.europa.eu/transparency/regexpert/index.cfm?do=groupDetail.groupDetailDoc&id=34592&no=1>. Accessed July 24, 2020.
- [3] Zhang X, Myhrvold NP, Hausfather Z, Caldeira K. Climate benefits of natural gas as a bridge fuel and potential delay of near-zero energy systems. *Appl Energy* 2016 Apr;1(167):317–22. <https://doi.org/10.1016/j.apenergy.2015.10.016>.
- [4] Faramawy S, Zaki T, Sakr AE. Natural gas origin, composition, and processing: a review. *J Nat Gas Sci Eng* 2016 Aug;1(34):34–54. <https://doi.org/10.1016/j.jngse.2016.06.030>.
- [5] IEA. Outlook for biogas and biomethane: Prospects for organic growth, IEA, Paris; 2020. <https://www.iea.org/reports/outlook-for-biogas-and-biomethane-prospects-for-organic-growth>. Accessed July 29, 2020.
- [6] Karim GA. Dual-fuel diesel engines. CRC Press 2015:1–312. <https://doi.org/10.1201/b18163>.
- [7] Srinivasan KK, Agarwal AK, Krishnan SR, Mulone V. Natural gas engines: for transportation and power generation. Springer 2018 Nov 3. <https://doi.org/10.1007/978-981-13-3307-1>.
- [8] Wei L, Geng P. A review on natural gas/diesel dual fuel combustion, emissions and performance. *Fuel Process Technol* 2016 Feb;1(142):264–78. <https://doi.org/10.1016/j.fuproc.2015.09.018>.
- [9] Korakianitis T, Namasivayam AM, Crookes RJ. Natural-gas fueled spark-ignition (SI) and compression-ignition (CI) engine performance and emissions. *Prog Energy Combust Sci* 2011 Feb 1;37(1):89–112. <https://doi.org/10.1016/j.pecs.2010.04.002Get>.
- [10] Kahila H, Kaario O, Ahmad Z, Masouleh MG, Tekgül B, Larmi M, et al. A large-eddy simulation study on the influence of diesel pilot spray quantity on methane-air flame initiation. *Combust Flame* 2019 Aug;1(206):506–21. <https://doi.org/10.1016/j.combustflame.2019.05.025>.
- [11] Ushakov S, Stenens D, Einang PM. Methane slip from gas fuelled ships: a comprehensive summary based on measurement data. *J Mar Sci Technol* 2019 Dec; 1:1–8. <https://doi.org/10.1007/s00773-018-00622-z>.
- [12] Anderson M, Salo K, Fridell E. Particle-and gaseous emissions from an LNG powered ship. *Environ Sci Technol* 2015 Oct 20;49(20):12568–75. <https://doi.org/10.1021/acs.est.5b02678>.
- [13] Kakaee AH, Paykani A, Ghajar M. The influence of fuel composition on the combustion and emission characteristics of natural gas fueled engines. *Renew Sustain Energy Rev* 2014 Oct;1(38):64–78. <https://doi.org/10.1016/j.rser.2014.05.080>.
- [14] Caillol C, Delorme T, Denis P, Berardi G, Porterie B. A combustion model for analyzing the effects of natural gas composition on the operation of a spark ignition engine. *SAE Technical Paper*; 2002 Jul 9. <https://doi.org/10.4271/2002-01-2236>.
- [15] Liu J, Dumitrescu CE. Numerical investigation of methane number and Wobbe index effects in lean-burn natural gas spark-ignition combustion. *Energy Fuels* 2019 Apr 15;33(5):4564–74. <https://doi.org/10.1021/acs.energyfuels.8b04463>.
- [16] Huang J, Bushe WK. Experimental and kinetic study of autoignition in methane/ethane/air and methane/propane/air mixtures under engine-relevant conditions. *Combust Flame* 2006 Jan 1;144(1–2):74–88. <https://doi.org/10.1016/j.combustflame.2005.06.013>.
- [17] Aul CJ, Metcalfe WK, Burke SM, Curran HJ, Petersen EL. Ignition and kinetic modeling of methane and ethane fuel blends with oxygen: a design of experiments approach. *Combust Flame* 2013 Jul 1;160(7):1153–67. <https://doi.org/10.1016/j.combustflame.2013.01.019>.
- [18] Healy D, Curran HJ, Simmie JM, Kalitan DM, Zinner CM, Barrett AB, et al. Methane/ethane/propane mixture oxidation at high pressures and at high, intermediate and low temperatures. *Combust Flame* 2008 Nov 1;155(3):441–8. <https://doi.org/10.1016/j.combustflame.2008.07.003>.
- [19] Nilsson EJ, van Sprang A, Larfeldt J, Konnov AA. The comparative and combined effects of hydrogen addition on the laminar burning velocities of methane and its blends with ethane and propane. *Fuel* 2017 Feb;1(189):369–76. <https://doi.org/10.1016/j.fuel.2016.10.103>.
- [20] Nilsson EJ, van Sprang A, Larfeldt J, Konnov AA. Effect of natural gas composition on the laminar burning velocities at elevated temperatures. *Fuel* 2019 Oct;1(253): 904–9. <https://doi.org/10.1016/j.fuel.2019.05.080>.
- [21] Mikulski M, Wierzbicki S. Numerical investigation of the impact of gas composition on the combustion process in a dual-fuel compression-ignition engine. *J Nat Gas Sci Eng* 2016 Apr;1(31):525–37. <https://doi.org/10.1016/j.jngse.2016.03.074>.
- [22] Wu Z, Rutland CJ, Han Z. Numerical evaluation of the effect of methane number on natural gas and diesel dual-fuel combustion. *Int J Engine Res* 2019 Apr;20(4): 405–23. <https://doi.org/10.1177/1468087418758114>.
- [23] Kakaee AH, Rahnama P, Paykani A. Influence of fuel composition on combustion and emissions characteristics of natural gas/diesel RCCI engine. *J Nat Gas Sci Eng* 2015 Jul;1(25):58–65. <https://doi.org/10.1016/j.jngse.2015.04.020>.
- [24] Ahmad Z, Kaario O, Cheng Q, Larmi M. Impact of ethane enrichment on diesel-methane dual-fuel combustion. *SAE Technical Paper*; 2020 Apr 14. <https://doi.org/10.4271/2020-01-0305>.
- [25] McTaggart-Cowan GP, Rogak SN, Munshi SR, Hill PG, Bushe WK. The influence of fuel composition on a heavy-duty, natural-gas direct-injection engine. *Fuel* 2010 Mar 1;89(3):752–9. <https://doi.org/10.1016/j.fuel.2009.10.007>.

- [26] Richards P. 'Automotive Fuels Reference Book. ISBN: 978-0-7680-0638-4. SAE International; 2014. <https://www.sae.org/publications/books/content/r-297/>.
- [27] Heywood JB. Internal combustion engine fundamentals. McGraw-Hill; 1998. p. (p.930). <https://doi.org/10.1036/007028637X>.
- [28] Ahmad Z, Kaario O, Qiang C, Vuorinen V, Larmi M. A parametric investigation of diesel/methane dual-fuel combustion progression/stages in a heavy-duty optical engine. *Appl Energy* 2019 Oct;1(251):113191. <https://doi.org/10.1016/j.apenergy.2019.04.187>.
- [29] Cantera DG. An object-oriented software toolkit for chemical kinetics, thermodynamics, and transport processes. 2012. Version 2.2. 1," Cantera Dev. Warrenton, 2016.
- [30] Karimkashi S, Kahila H, Kaario O, Larmi M, Vuorinen V. A numerical study on combustion mode characterization for locally stratified dual-fuel mixtures. *Combust Flame* 2020 Apr;1(214):121–35. <https://doi.org/10.1016/j.combustflame.2019.12.030>.
- [31] Zeldovich YB. Regime classification of an exothermic reaction with nonuniform initial conditions. *Combust Flame* 1980 Oct 1;39(2):211–4. [https://doi.org/10.1016/0010-2180\(80\)90017-6](https://doi.org/10.1016/0010-2180(80)90017-6).
- [32] Kayadelen HK. Effect of natural gas components on its flame temperature, equilibrium combustion products and thermodynamic properties. *J Nat Gas Sci Eng* 2017 Sep;1(45):456–73. <https://doi.org/10.1016/j.jngse.2017.05.023>.
- [33] Bolt JA, Henein NA. The effect of some engine variables on ignition delay and other combustion phenomena in a diesel engine. In: Proceedings of the institution of mechanical engineers, conference proceedings 1969 Sep (Vol. 184, No. 10, p. 130–6). Sage UK: London, England: SAGE Publications. [https://doi.org/10.1243/PIME\\_CONF\\_1969\\_184\\_327\\_02](https://doi.org/10.1243/PIME_CONF_1969_184_327_02).
- [34] Cheng Q, Ahmad Z, Kaario O, Martti L. Cycle-to-cycle variations of dual-fuel combustion in an optically accessible engine. *Appl Energy* 2019 Nov;15(254): 113611. <https://doi.org/10.1016/j.apenergy.2019.113611>.
- [35] Mastorakos E. Ignition of turbulent non-premixed flames. *Prog Energy Combust Sci* 2009 Feb 1;35(1):57–97. <https://doi.org/10.1016/j.pecs.2008.07.002>.
- [36] Bilger RW, Stårner SH, Kee RJ. On reduced mechanisms for methane-air combustion in nonpremixed flames. *Combust Flame* 1990 May 1;80(2):135–49. [https://doi.org/10.1016/0010-2180\(90\)90122-8](https://doi.org/10.1016/0010-2180(90)90122-8).
- [37] Frassoldati A, D'Errico G, Lucchini T, Stagni A, Cuoci A, Faravelli T, et al. Reduced kinetic mechanisms of diesel fuel surrogate for engine CFD simulations. *Combust Flame* 2015 Oct 1;162(10):3991–4007. <https://doi.org/10.1016/j.combustflame.2015.07.039>.
- [38] Kahila H, Wehrfritz A, Kaario O, Vuorinen V. Large-eddy simulation of dual-fuel ignition: diesel spray injection into a lean methane-air mixture. *Combust Flame* 2019 Jan;1(199):131–51. <https://doi.org/10.1016/j.combustflame.2018.10.014>.
- [39] Petersen EL, Hall JM, Smith SD, de Vries J, Amadio AR, Crofton MW. Ignition of lean methane-based fuel blends at gas turbine pressures. <https://doi.org/10.1115/1.2720543>.
- [40] Karimkashi S, Kahila H, Kaario O, Larmi M, Vuorinen V. Numerical study on tri-fuel combustion: Ignition properties of hydrogen-enriched methane-diesel and methanol-diesel mixtures. *Int J Hydrogen Energy* 2020 Feb 7;45(7):4946–62. <https://doi.org/10.1016/j.ijhydene.2019.12.033>.